Supporting Information

Soft, wearable, microfluidic system for fluorometric analysis of loss of amino acids through eccrine sweat

Seunghee H. Cho[a, b, c, d], Soongwon Cho[a, b], Zengyao Lv[e], Yurina Sekine[f], Shanliangzi Liu[a, b], Mingyu Zhou[a, g], Ravi F. Nuxoll[a, h, i], Evangelos E. Kanatzidis[a], Roozbeh Ghaffari[a, b, g, j], Donghwan Kim[c, d], Yonggang Huang[a, e, h, k], and John A. Rogers[a, b, g, h, l]*

[a.] Querrey-Simpson Institute for Bioelectronics, Northwestern University, Evanston, IL 60208, USA
[b.] Center for Bio-Integrated Electronics, Northwestern University, Evanston, IL, 60208, USA
[c.] School of Chemical Engineering, Sungkyunkwan University, 2066 Seobu-ro, Suwon, 16419, Republic of Korea.
[d.] Biomedical Institute for Convergence at SKKU (BICS), Sungkyunkwan University, 2066 Seobu-ro, Suwon, 16419, Republic of Korea.
[e.] Department of Civil and Environmental Engineering, Northwestern University, Evanston, IL 60208, USA
[f.] Materials Sciences Research Center, Japan Atomic Energy Agency, Tokai, Ibaraki 319-1195, Japan
[g.] Department of Biomedical Engineering, Northwestern University, Evanston, IL 60208, USA
[h.] Department of Materials Science and Engineering, Northwestern University, Evanston, IL 60208, USA
[i.] Department of Physics and Astronomy, Northwestern University, Evanston, IL 60208, USA
[j.] Epicore Biosystems, Cambridge, MA, 02139, USA
[k.] Department of Mechanical Engineering, Northwestern University, Evanston, IL 60208, USA
[l.] Department of Neurological Surgery, Northwestern University Feinberg School of Medicine, Chicago, IL 60611, USA

*Corresponding author: jrogers@northwestern.edu

Supplementary note 1: Capillary bursting valve design

CBVs are designed with specific bursting pressures at which fluid is allowed to pass through, based on the Young-Laplace equation (**Equation S1**), where σ is the surface tension of the liquid, θ is the contact angle of the channel, β is the diverging angle of the channel, b is the width of the channel, and h is the height of the channel..

$$Bursting\ pressure\ (BP) = -2\sigma\left[\frac{\cos\left(min(\theta+\beta,180°)\right)}{b} + \frac{\cos\theta}{h}\right] \quad \text{(S1)}$$

Supplementary note 2: Computational fluid dynamics (CFD) simulations

The creation, evolution and dissolution of the water-air interface are described by convective Cahn–Hilliard equation (Equation S2),[1, 2] where ϕ is the order parameter representing the relative concentration of the two components, and M is the mobility.[3] In Equation S3, M_c is the characteristic mobility, and $\varepsilon_{\mathrm{pf}}$ is a capillary width that scales with the thickness of the diffuse interface. The chemical potential μ is given by Equation S4,[1] where λ is the mixing energy density.

$$\rho\frac{\partial\phi}{\partial t} + \boldsymbol{v}\cdot\nabla\phi = \nabla\cdot(M\nabla\mu) \quad \text{(S2)}$$

$$M = M_c\varepsilon_{\mathrm{pf}}^2 \quad \text{(S3)}$$

$$\mu = \frac{\lambda}{\varepsilon_{\mathrm{pf}}^2}\left[(\phi^2-1)\phi - \varepsilon_{\mathrm{pf}}^2\nabla^2\phi\right] \quad \text{(S4)}$$

The flow in the device is described by the incompressible Navier-Stokes equation (Equation S5, S6) with the shallow channel approximation[4-6] and a phase field-dependent surface force[2], where $\boldsymbol{v}$ is the velocity vector, p is the pressure, η is the viscosity, ρ is the fluid density, d is the channel thickness.

$$\rho \frac{\partial \boldsymbol{v}}{\partial t} + \rho(\boldsymbol{v} \cdot \nabla)\boldsymbol{v} = \nabla \cdot \{-p\boldsymbol{I} + \eta[\nabla \boldsymbol{v} + (\nabla \boldsymbol{v})^T]\} - 12\frac{\eta \boldsymbol{v}}{d^2} + \mu \nabla \phi \quad \text{(S5)}$$

$$\nabla \cdot \boldsymbol{v} = 0 \quad \text{(S6)}$$

The surface tension coefficient σ is equal to the integral of the free energy density across the interface (Equation S7).[3, 7]

$$\sigma = \frac{2\sqrt{2}}{3}\frac{\lambda}{\varepsilon_{\mathrm{pf}}} \quad \text{(S7)}$$

Numerical simulations were conducted using COMSOL Multiphysics™, employing triangular mesh elements for all computational analyses. A refined mesh with feature sizes smaller than 1/6 of the channel width was adopted to ensure accuracy. The numerical solver dynamically controlled time step sizes through backward differentiation formulas (BDFs), with initial step sizes kept small to prevent singularity. During initialization, the interface equation was solved under stationary conditions to ensure a smooth initial interface transition. The boundary conditions were set to no-slip, where the inlet end was set to the water phase and outlet pressure was maintained at 0. Water and air were modeled as Newtonian fluids with the following parameters: ρ_w =997kg/m^3, η_w=0.0010016Pa·s for liquid water; ρ_a=1.204kg/m^3, η_a=1.825×10^{-5}Pa·s for air. The interfacial tension was 72.74 mN/m. The contact angle of PDMS[8] was 125°.

Supplementary note 3: Smartphone-based imaging module

Fig. S2 summarizes the key features of the setup and demonstrates the process flow for analysis. For the smartphone mount, a miniature dark box defined using a 3D printing process (Form3+, Formlabs, USA) is attached to a commercially available lens mount (Lens kit, Xenvo) adopting a clip-like configuration **(Fig. S2a)**. Excitation filters (Scotchcal™ graphic film, 3632-87; 3M, MN,

USA) were attached to the smartphone flash to enable suitable excitation for the fluorometric analysis using standard smartphone camera LED flash functions (**Fig. S2b-c**). The filter passes light with a narrow range of wavelengths (531 ± 30 nm) from the smartphone LED flash for excitation of the fluorescent probes (Excitation wavelengths 535 – 538 nm), as shown in **Fig. S3**.

For quantitative analysis of amino acids, the user can capture the fluorescent images of the wearable device (**Fig. S2d-e**). Image analysis software can be utilized to extract the intensity of reference (I_{Ref}) and sample (I_{Sample}) microreservoirs (**Fig. S2f**) and calculate the amino acid concentrations based on **Equation S7**.

$$Concentration \propto Normalized\ Intensity = \frac{I_{Ref}}{I_{Sample}} \quad \text{(S7)}$$

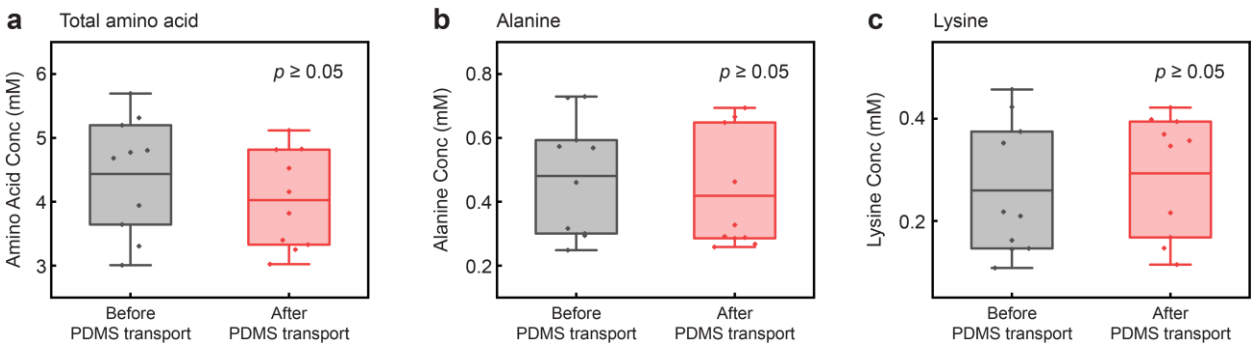

Fig. S1. PDMS absorption tests. Analysis of sweat samples before and after transport through PDMS microfluidic channels for total amino acid (a), alanine (b), and lysine (c).

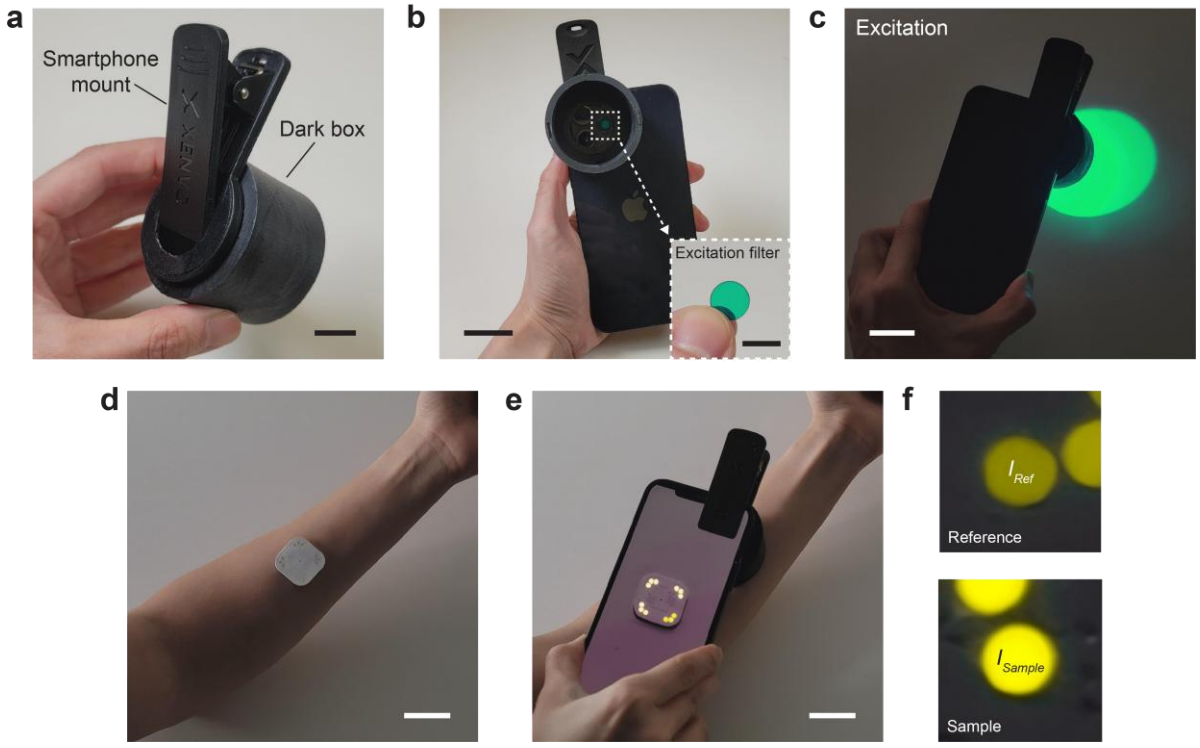

Fig. S2. **Smartphone-based imaging module.** (a) Smartphone mount with dark box. Scale bar, 1 cm (b) Smartphone-based imaging module with excitation filter placed over flash. Scale bar, 3 cm. Inset scale bar, 5 mm. (c) Excitation using smartphone flash. Scale bar, 3 cm. (d, e) Fluorometric analysis of the wearable device using the smartphone-based imaging module. Scale bars, 3 cm. (f) Measurement of reference and sample fluorescence intensities for quantification.

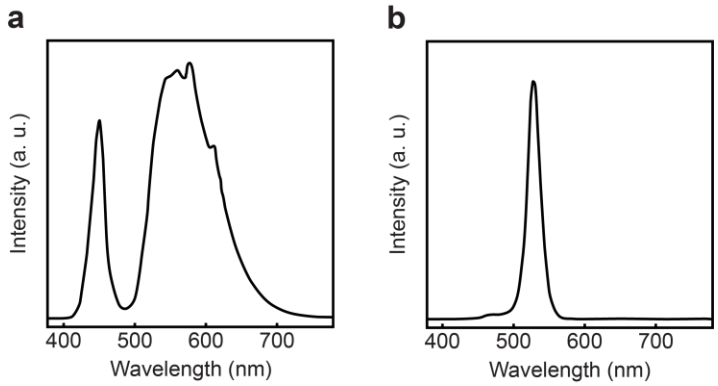

Fig. S3. **Excitation filter characterization.** (a) Spectra of smartphone LED flash. (b) Spectra of smartphone LED flash with excitation filter.

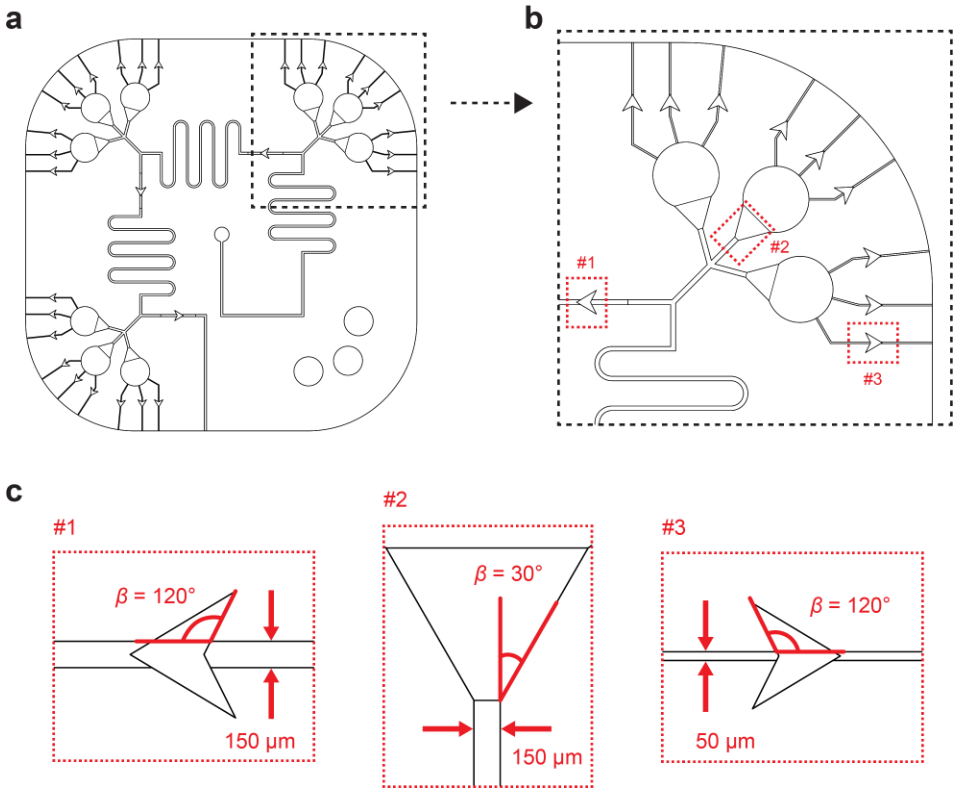

Fig. S4. **Schematic illustration of the microfluidic system.** Detailed schematics for the entire microfluidic device (a) and unit cell (b) of the microfluidic system. (c) Magnified view of each CBV labeled with relative parameters.

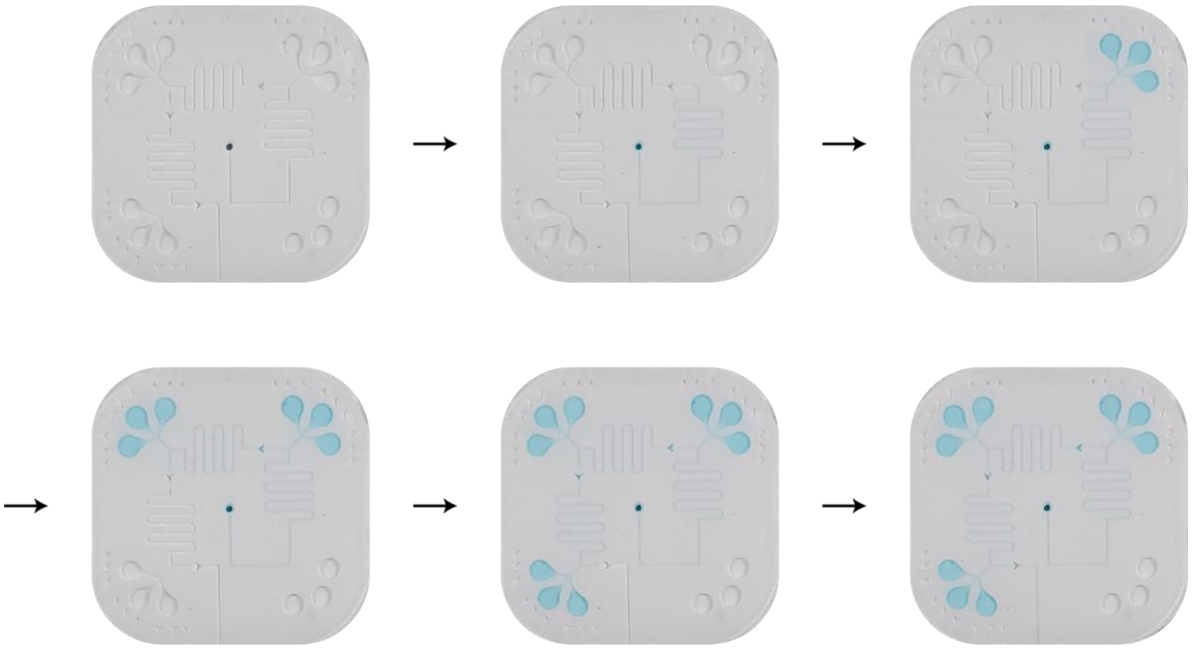

Fig. S5. Images of microfluidic system showing simultaneous filling of three sets of grouped microreservoirs.

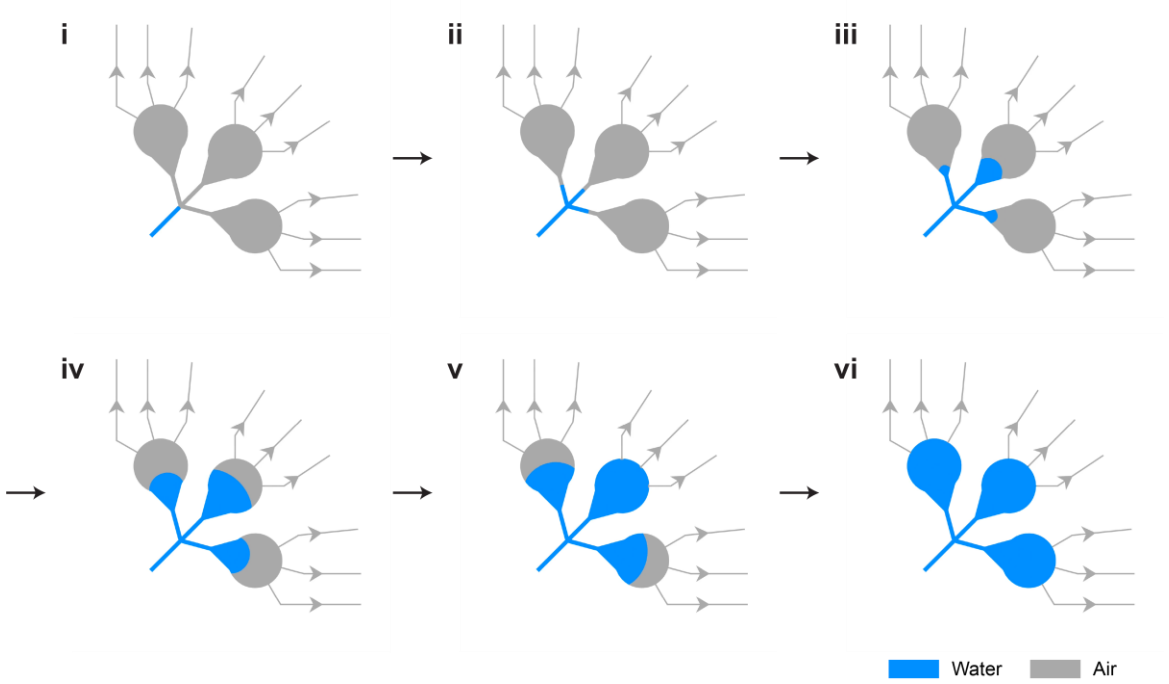

Fig. S6. **Computational fluid dynamics simulation results.** Simulated progression of water/air interface showing the simultaneous filling of grouped reservoirs.

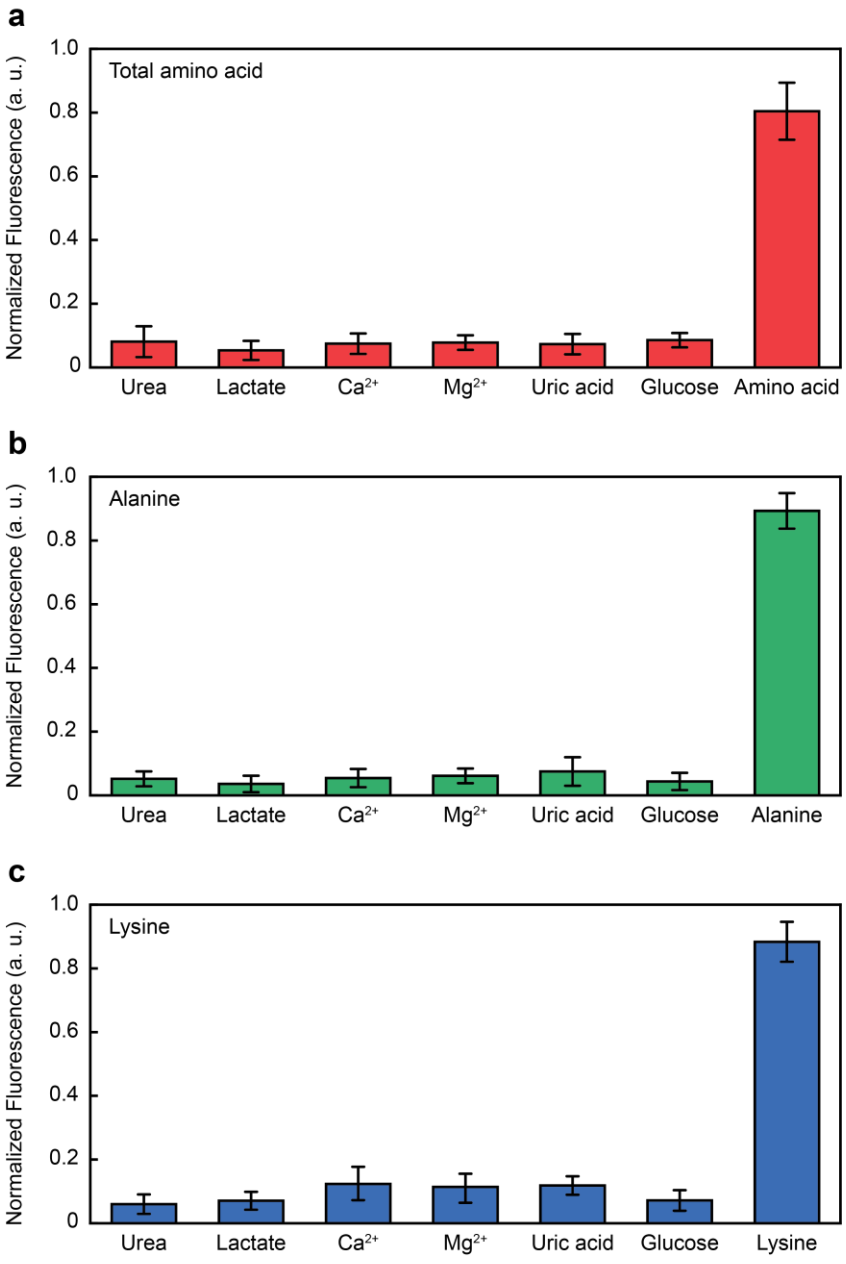

Fig. S7. Fluorometric results from each enzymatic assay targeting total amino acid (a), alanine (b), and lysine (c), when exposed to potential interferents (10 mM urea, 10mM lactate, 0.5 mM Ca^{2+}, 0.5 mM Mg^{2+}, 10 mM uric acid, and 10 mM glucose) and target amino acids (10 mM total amino acid, 2 mM alanine, and 2 mM lysine).

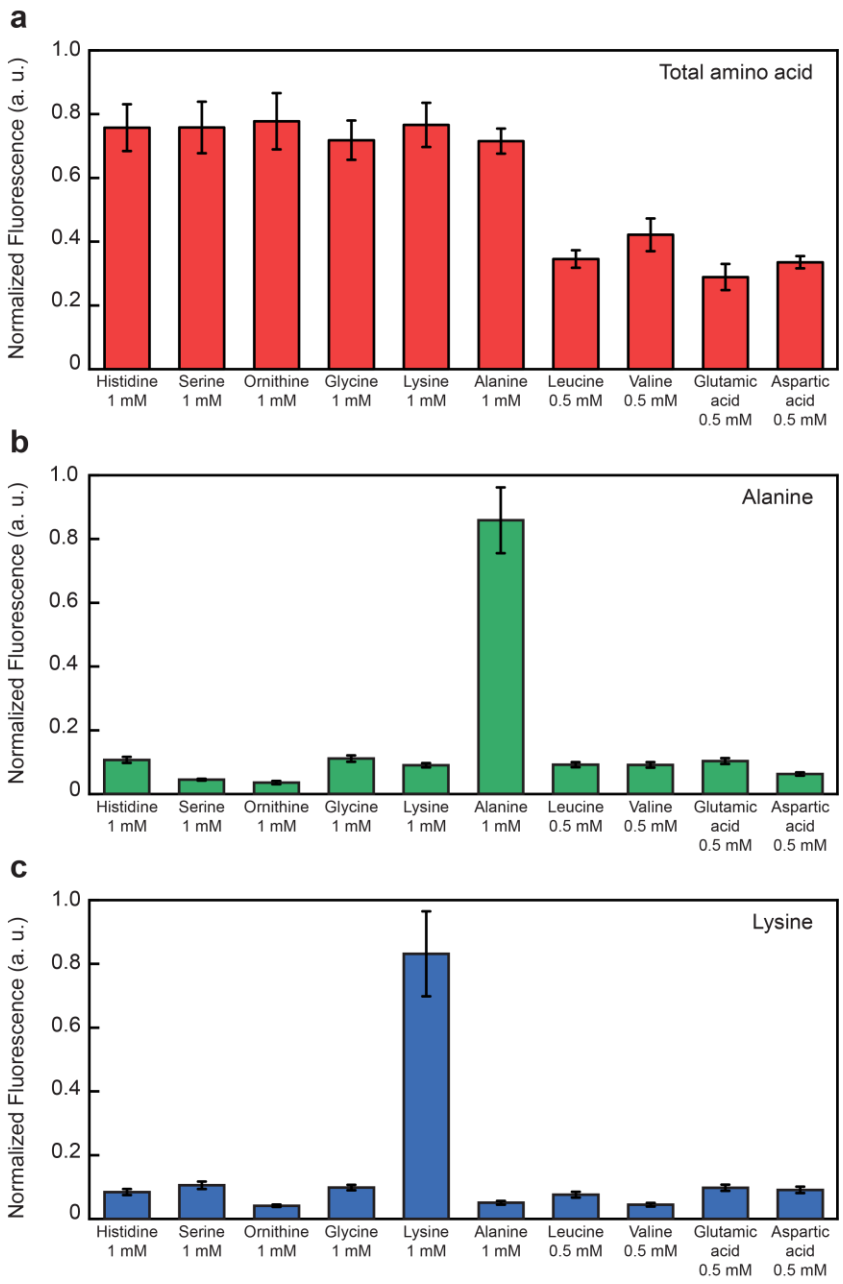

Fig. S8. Cross-reactivity between amino acids. Fluorometric results from each enzymatic assay targeting total amino acid (a), alanine (b), and lysine (c), when exposed to various amino acids (1 mM histidine, 1 mM serine, 1 mM ornithine, 1 mM glycine, 1 mM lysine, 1 mM alanine, 0.5 mM leucine, 0.5 mM valine, 0.5 mM glutamic acid, and 0.5 mM aspartic acid).

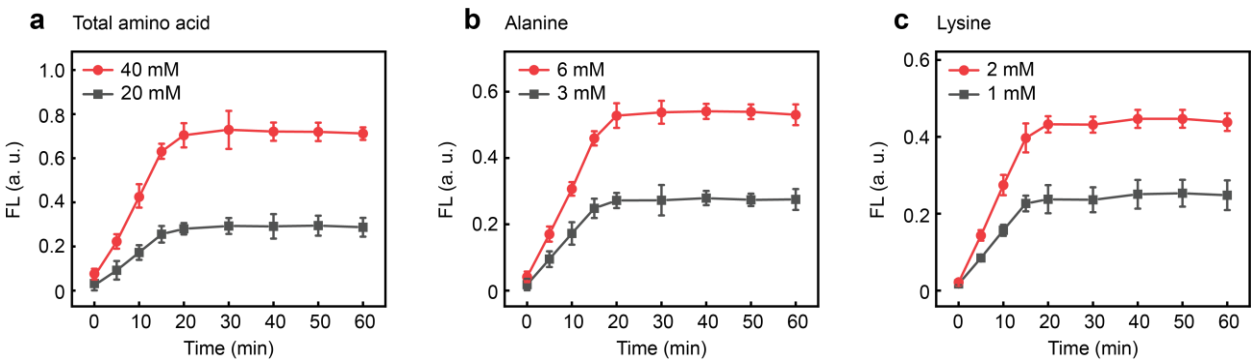

Fig. S9. Fluorometric results for the enzymatic assays as a function of reaction time for total amino acid (a), alanine (b), and lysine (c).

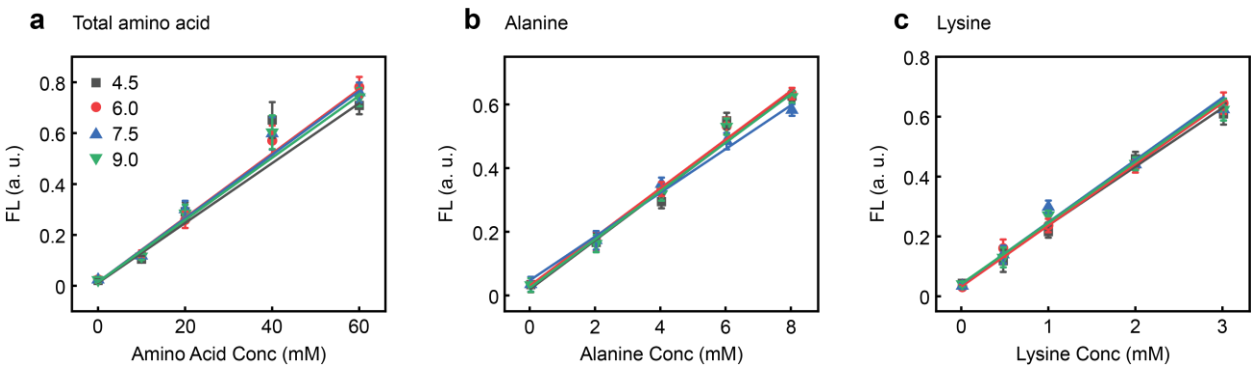

Fig. S10. Fluorometric results for the enzymatic assays at various pH for total amino acid (a), alanine (b), and lysine (c).

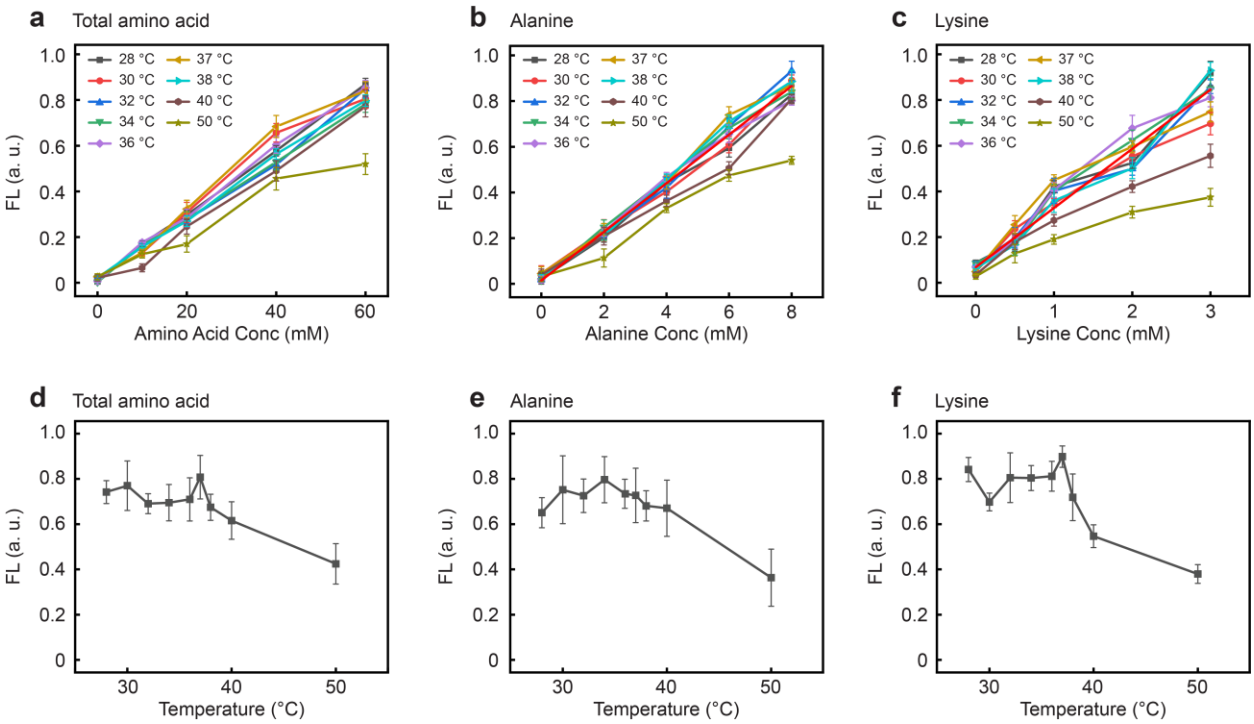

Fig. S11. Temperature dependency of enzymatic assays. Fluorometric results from enzymatic assays for total amino acid (a), alanine (b), and lysine (c) of various concentrations and temperatures (28-50 °C). Fluorometric results for 20 mM total amino acid (d), 2 mM alanine (e), and 1 mM lysine (f) at various temperatures (28-50 °C).

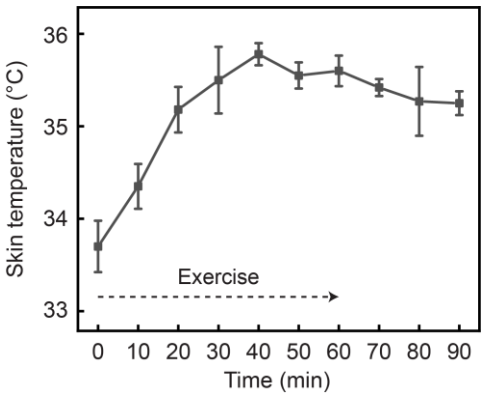

Fig. S12. Skin temperature measured pre-exercise, during a 60 min exercise on stationary bike, and post-exercise recovery.

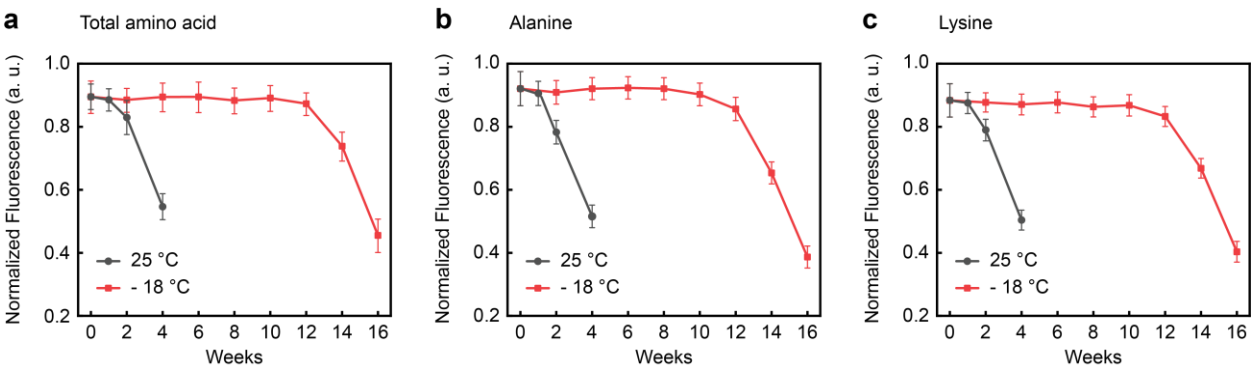

Fig. S13. Fluorometric results for the enzymatic assays as a function of storage time at temperatures 25 °C and -18 °C for total amino acid (a), alanine (b), and lysine (c).

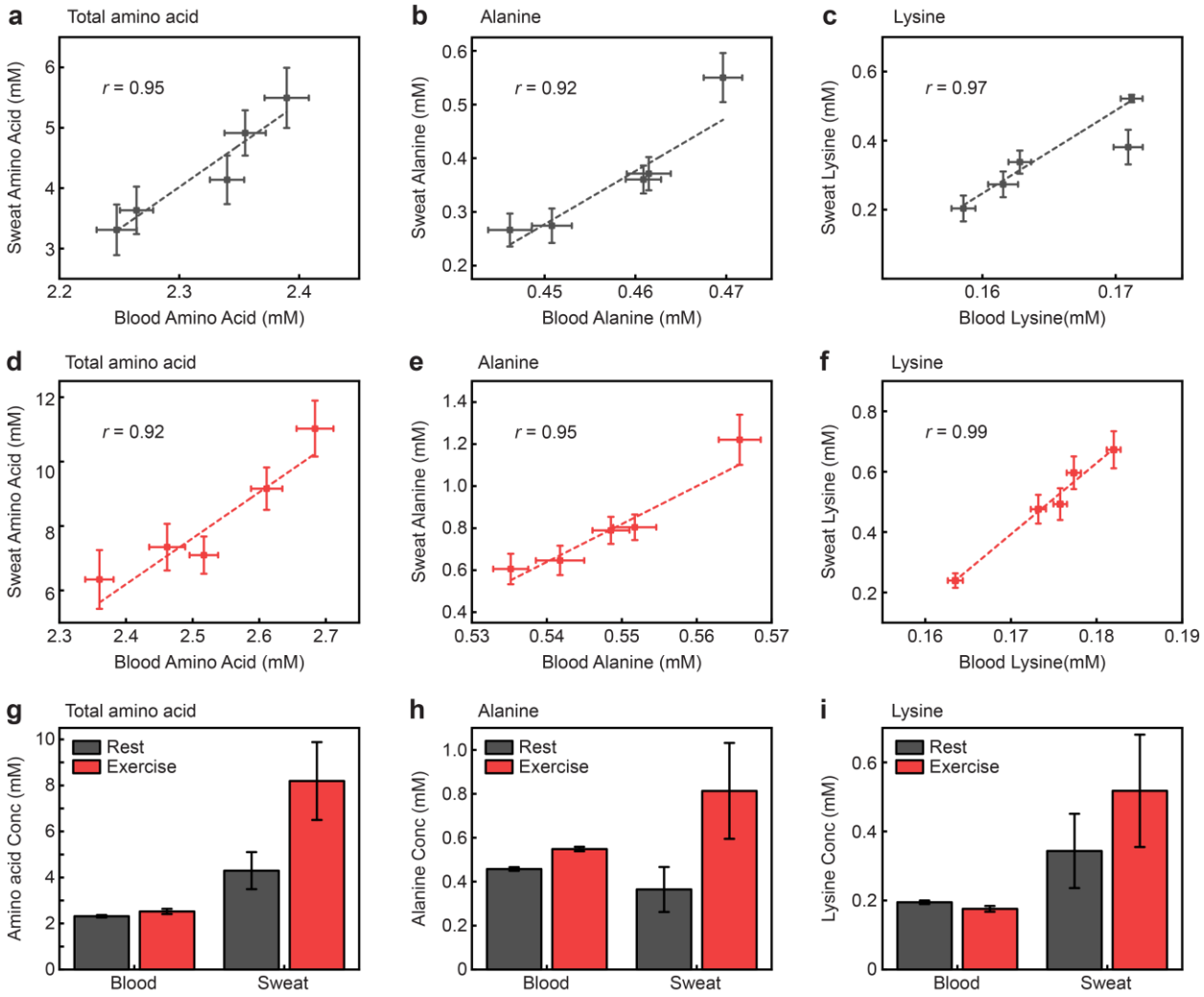

Fig. S14. Correlation between amino acid concentrations from blood and sweat. Analysis of blood and sweat samples taken during rest (a-c), after 30 min exercise on a stationary bike (d-f), and comparison results (g-i) for total maino acid (a, d, g), alanine (b, e, h), and lysine (c, f, i) (n = 5).

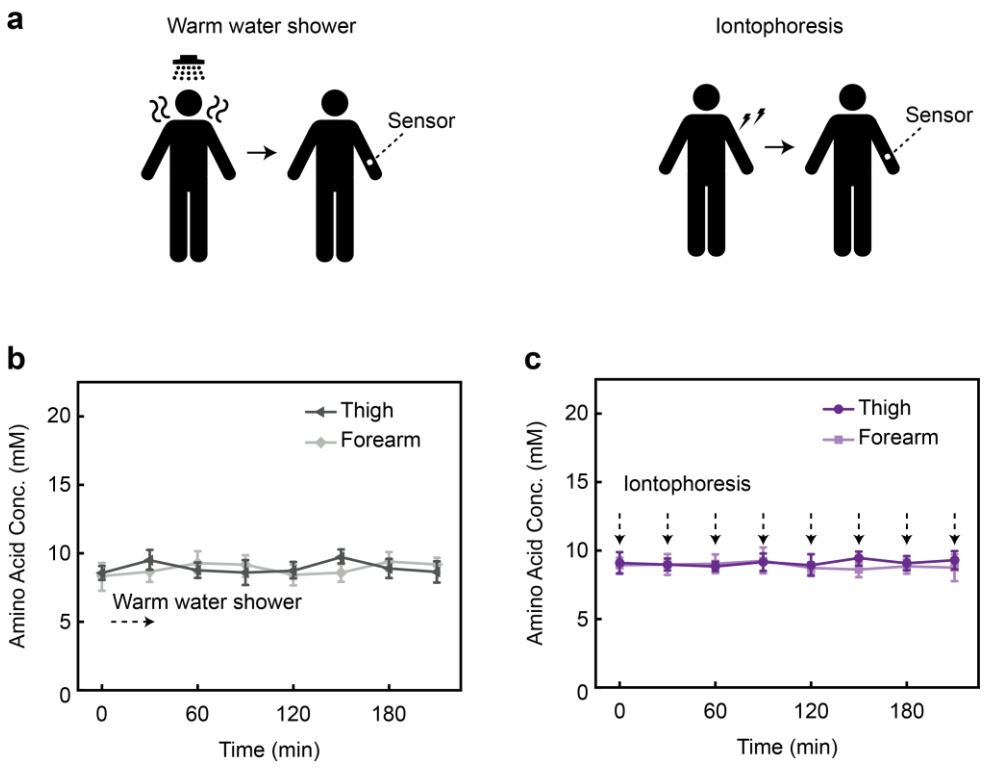

Fig. S15. (a) Protocol for human subject studies involving sweat induction methods of warm water shower and iontophoresis. (b, c) Time-dynamic analysis of total amino acid in sweat induced by warm water shower (b) and iontophoresis (c) from the thigh and forearm.

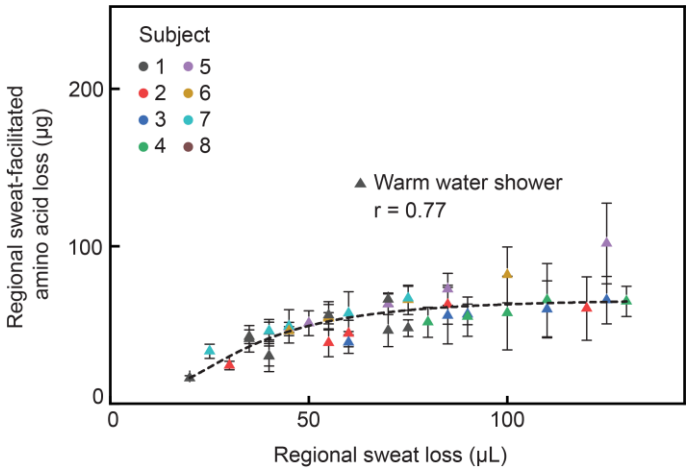

Fig. S16. Correlation of total amino acid loss and total sweat loss after a warm water shower from various body locations (n = 8).

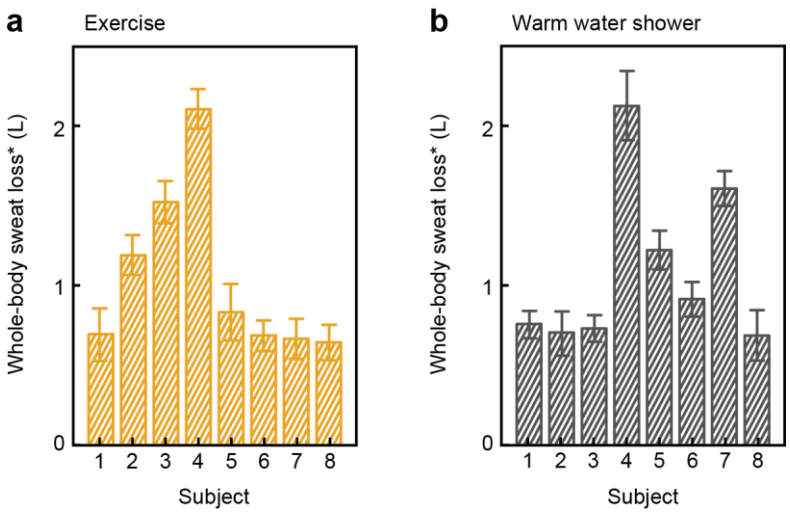

Fig. S17. Whole body sweat loss estimates for exercise (a) and warm water shower (b). (n = 8)

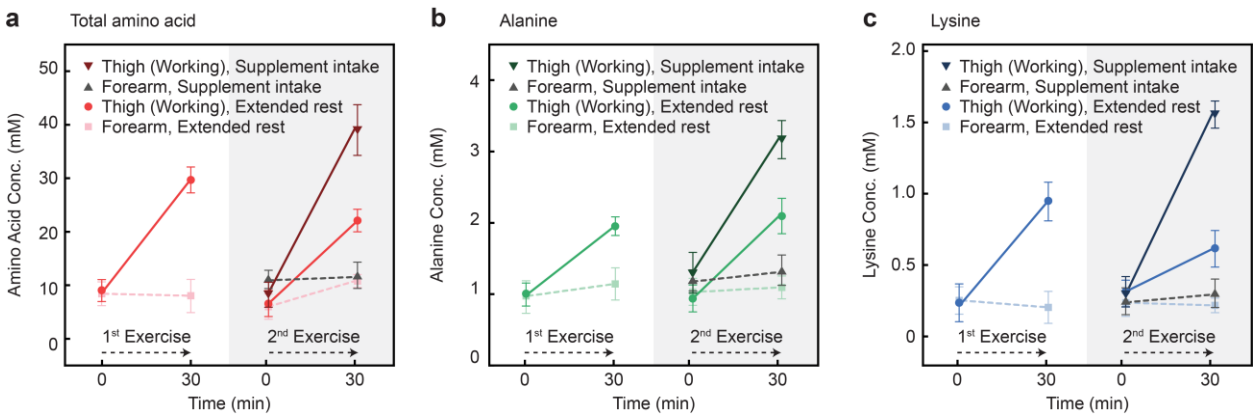

Fig. S18. Extended recovery periods. Sweat amino acid levels from a working region (thigh) and non-working region (forearm) during two exercise sessions separated by an extended 4-hour recovery period involving either only rest or rest accompanied with supplement intake, for total amino acid (a), alanine (b), and lysine (c) (n = 3).

Sensor type	Detection method	Amino acid	Essential/ Non-essential	LOD	Reference
Electrochemical	Oxidation	Tyrosine	Non-essential	3.6 μM	3
Electrochemical	Molecular imprinting	Tryptophan	Essential	0.67 μM	4
Electrochemical	Enzymatic reaction	Glycine	Non-essential	7.9 μM	5
Colorimetric	Enzymatic reaction	Leucine	Essential	6.0 mg/L	6
	Enzymatic reaction	Isoleucine		6.2 mg/L	
	Enzymatic reaction	Valine		7.0 mg/L	
Colorimetric	Ionic reaction	Cysteine	Essential	0.5 μM	7
	Ionic reaction	Histidine		1.5 μM	
Fluorometric	Enzymatic reaction	Total amino acid	Essential, Non-essential, & Total	3.68 μM	This work
	Enzymatic reaction	Alanine		0.49 μM	
	Enzymatic reaction	Lysine		0.13 μM	

Table S1. **Wearable amino acid sensors.**

CBV	**#1**	**#2**	**#3**
σ (mN/m)	72.74	72.74	72.74
θ (º)	125.00	125.00	125.00
β (º)	120.00	30.00	120.00
***b* (µm)**	150.00	150.00	50.00
***h* (µm)**	75.00	400.00	25.00
BP (Pa)	2,082.74	1,087.76	6,248.21

Table S2. Calculated bursting pressures (BP) of the three CBVs shown in Figure SXc and their parameters.

Component	Cost per sensor (USD)
Total amino acid assay reagents	0.545
Alanine assay reagents	0.273
Lysine assay reagents	0.273
Cellulose paper	0.002
Microfluidic layer (PDMS)	0.231
Total cost	1.324

Table S3. Production cost of wearable device for fluorometric amino acid sensor.

	Surface area coefficient
Forehead	0.07
Chest	0.175
Lower back	0.175
Forearm	0.095
Thigh	0.39

Table S4. Surface area coefficients for whole-body calculations.

References

1. V. E. Badalassi, H. D. Ceniceros, and S. Banerjee, *J. Comput. Phys*, 2003, **190**(2), 371
2. M. E. Gurtin, D. Polignone, and J. Viñals, *Math. Models Methods Appl. Sci.*, 1996, **6**(06), 815
3. H. A. Akhlaghi Amiri and A. A. Hamouda, *Int. J. Multiph. Flow*, 2013, **52**, 22
4. M. Stoll, F. M. Huber, M. Trumm, F. Enzmann, D. Meinel, A. Wenka, E. Schill, and T. Schäfer, *J. Contam. Hydrol.*, 2019, **221**, 82
5. M. Coblyn, A. Truszkowska, and G. Jovanovic, *J. Flow Chem.*, 2016, **6**, 53
6. H. Bruus, *Theoretical Microfluidics (Vol 18)*, Oxford University Press, 2007
7. R. S. Qin and H. K. Bhadeshia, *Mater. Sci. Technol.*, 2010, **26**(7), 803
8. J. Choi, Y. Xue, W. Xia, T. R. Ray, J. T. Reeder, A. J. Bandodkar, D. Kang, S. Xu, Y. Huang, and J. A. Rogers, *Lab Chip*, 2017, **17**(15), 2572
9. Y. Yang, Y. Song, X. Bo, J. Min, O.S. Pak, L. Zhu, M. Wang, J. Tu, A. Kogan, H. Zhang, T.K. Hsiai, Z. Li, and W. Gao, *Nat. Biotech.*, 2020, **38**(2), 217
10. Z. Xu, Y. Liu, M. Lv, X. Qiao, G. C. Fan, and X. Luo, *Anal. Chim. Acta*, 2023, **1283**, 341948
11. Q. Wang, A. Molinero-Fernandez, A. Casanova, J. Titulaer, J. C. Campillo-Brocal, Å. Konradsson-Geuken, G. A. Crespo, and M. Cuartero. *Anal. Chem.*, 2022, **94**(34), 11856
12. S. Teepoo, T. Sannok, S. Arsawiset, and S. Sansenya, *Food Chem.*, 2023. **405**, 134560
13. F. Razavi and H. Khajehsharifi, *Chem. Pap.*, 2021. **75**, 3401